Published as: *IEEE Trans Biomed Circuits Syst*. 2011 October ; 5(5): 420–429.

# Biophysical Neural Spiking, Bursting, and Excitability Dynamics in Reconfigurable Analog VLSI

**Theodore Yu[Student Member, IEEE]**,
Department of Electrical and Computer Engineering, Jacobs School of Engineering and Institute of Neural Computation, University of California San Diego, La Jolla, CA 92093 USA

**Terrence J. Sejnowski[Fellow, IEEE]**, and
Division of Biological Sciences and Institute of Neural Computation, University of California San Diego, La Jolla, CA 92093 USA and also with the Howard Hughes Medical Institute, Salk Institute, La Jolla, CA 92037 USA

**Gert Cauwenberghs[Fellow, IEEE]**
Department of Bioengineering, Jacobs School of Engineering and Institute of Neural Computation, University of California San Diego, La Jolla, CA 92093 USA

Theodore Yu: teyu@ucsd.edu; Terrence J. Sejnowski: terry@salk.edu; Gert Cauwenberghs: gert@ucsd.edu

## Abstract

We study a range of neural dynamics under variations in biophysical parameters underlying extended Morris–Lecar and Hodgkin–Huxley models in three gating variables. The extended models are implemented in *NeuroDyn*, a four neuron, twelve synapse continuous-time analog VLSI programmable neural emulation platform with generalized channel kinetics and biophysical membrane dynamics. The dynamics exhibit a wide range of time scales extending beyond 100 ms neglected in typical silicon models of tonic spiking neurons. Circuit simulations and measurements show transition from tonic spiking to tonic bursting dynamics through variation of a single conductance parameter governing calcium recovery. We similarly demonstrate transition from graded to all-or-none neural excitability in the onset of spiking dynamics through the variation of channel kinetic parameters governing the speed of potassium activation. Other combinations of variations in conductance and channel kinetic parameters give rise to phasic spiking and spike frequency adaptation dynamics. The *NeuroDyn* chip consumes 1.29 mW and occupies 3 mm × 3 mm in 0.5 $\mu$m CMOS, supporting emerging developments in neuromorphic silicon-neuron interfaces.

### Index Terms

Analog VLSI; biophysical neural dynamics; neuromorphic engineering; programmable channel kinetics; silicon neuron interfaces; spiking neuron models

## I. Introduction

Neuromorphic engineering, as an analysis by synthesis approach to computational neuroscience, is increasingly offering physical tools for studying the dynamics of complex neural systems [1]–[4]. While analog neural chips inherently have limited programming capability, recent designs have overcome this limitation by incorporating a large number of


Color versions of one or more of the figures in this paper are available online at http://ieeexplore.ieee.org.

parameters in a reconfigurable architecture [5]–[11]. This opens up opportunities in systematic studies of the dependence of the dynamics upon biophysical parameters. Iterative methods, such as gradient descent learning [12] and evolutionary algorithms [13]–[15] can then be applied to estimate the model parameters for biological inference.

Here we present such a study on a silicon biophysical neural model with wide-ranging membrane dynamics and channel kinetics [16] that, within the same architecture as illustrated in Fig. 1, extends the Hodgkin–Huxley (HH) and Morris-Lecar (ML) paradigms from tonic spiking to intrinsically bursting neural dynamics [17] and a variety of other neural dynamics. Neurons exhibit dynamics at a wide range of time scales. However, longer time scales extending beyond 100 ms have been neglected in silicon models. We include mechanisms at such longer time scales that provide network models with new computational abilities, including central pattern generation [18] and memory consolidation in thalamocortical networks [19].

One of the simplest neuron models, a leaky quadratic integrate-and-fire model by Izhikevich [20], uses just two dynamical variables and four parameters to generate 20 distinct types of neuronal dynamics. A further simplified model with linear membrane dynamics has been shown by Mihalas and Niebur [21] to generate an equivalent range of neuronal dynamics. Despite the success of these models to efficiently emulate rich dynamics in analog VLSI [22]–[25], the very compact state representation does not offer a direct biophysical interpretation of their parameters. Our work provides an alternative biophysically-based approach in an extended HH-ML formalism with generalized channel kinetics. We demonstrate a variety of neural dynamics through detailed control of the parameters governing the voltage-dependence profile of the opening and closing channel kinetic rates. Because each parameter is directly related to channel kinetics, the tuning of these parameters may provide insight into neuroscientific or clinical questions related to changes in, for instance, neuromodulators and pharmacological agents acting upon the modeled channels.

A variety of silicon neuron circuits have been proposed to implement models with varying degree of biophysical realism [26]. A parameterized library of biophysically-based analog operators in the HH model framework has been presented in [8]. A floating gate silicon neuron implementation also demonstrates a variety of neural dynamics and bifurcations [27].

Here we use *NeuroDyn* [28]–[31] as an experimental analog continuous-time platform to study parameterized biophysical neural dynamics over an extended range of time scales within a generalized HH-ML framework [32]. Fidelity between circuit simulation and measurement data, along with a low-power and compact circuit implementation, are key factors in utilizing a continuous-time analog VLSI emulation platform, such as *NeuroDyn*, as a versatile tool in neuromorphic modeling and silicon-neuron interfaces [33]–[35].

In [28] we demonstrated that the addition of a slow inactivation term to the ML neuron model results in bursting neural dynamics in the *NeuroDyn* analog VLSI implementation. Calculation of inter-spiking interval (ISI) for both simulated and measured bursting waveforms over the variation of a single conductance parameter $g_w$ governing calcium recovery show agreement in behavior between simulation and circuit measurement data.

Here we present, in addition to tonic spiking and intrinsically bursting dynamics, a wider range of neural dynamics including phasic spiking and spike-frequency adaptation within the same *NeuroDyn* analog VLSI implementation platform by systematic variation of parameters governing $Na^+$ and $K^+$ channel kinetics. We also present class 1 and class 2 neural excitability dynamics and show that variation of the dynamical voltage-dependent profile of $\tau_n$ governing $K^+$ inactivation results in an exchange between the two behaviors.

Calculation of ISI for both simulated and measured class 1 and class 2 neural excitability ramp responses show agreement in behavior between simulation and circuit measurement data.

## II. NeuroDyn Overview

The *NeuroDyn* system [28]–[31], illustrated in Fig. 1, consists of 4 neurons with Hodgkin–Huxley type membrane dynamics fully connected through 12 conductance-based synapses. All parameters are individually addressable and individually programmable and are biophysically-based governing the conductances, reversal potentials, and voltage-dependence of the channel kinetics. Each opening and closing channel kinetic rate is approximated with a 7-point spline regression function allowing for detailed control of the channel kinetics. These 14 parameters with two additional terms governing reversal potential and conductance per channel result in a total of 384 parameters each stored on-chip in a 10-bit DAC. Parameter fitting is achieved through rectified linear regression and iterative least squares residue correction. Scalable neural and synaptic arrays can be implemented by abstracting the desired dynamics of the neurons and synapses models and pooling together parameter control from individual to populations of neurons.

The analog VLSI design of the *NeuroDyn* system, and preliminary experimental results were presented in [29]. First results on coupled neural dynamics with inhibitory synapses were reported in [30]. Details on the circuit implementation and complete experimental characterization of the neural and synaptic circuits, as well as presentation of calibration and parameter fitting procedures to align neural and synaptic characteristics from models or recorded data onto the digitally programmable analog hardware are presented in [31]. In the following sections we focus on the extension of the HH model implemented in *NeuroDyn* to accommodate generalized dynamics over extended time scales.

## III. Methodology

### A. Membrane Dynamics

The Hodgkin–Huxley membrane dynamics [36] describe neural dynamics as a sum of conductance-based channel currents. Gating variables *m*, *h*, and *n* describe the voltage-dependent dynamical profiles of each channel and are described by

$$C_{mem}\frac{dV_i}{dt} = -I_{Na_i} - I_{K_i} - I_{L_i} - I_{syn_{ij}} \tag{1}$$

where $i, j = 0 \ldots 3$, and

$$\begin{aligned} I_{Na_i} &= m_i^3 h_i g_{Na_i}(V_i - E_{Na_i}) \\ I_{K_i} &= n_i^4 g_{K_i}(V_i - E_{K_i}) \\ I_{L_i} &= g_{L_i}(V_i - E_{L_i}). \\ I_{syn_{ij}} &= r_{ij} g_{syn_{ij}}(V_i - E_{syn_{ij}}). \end{aligned}$$

In order to emulate bursting neural dynamics, the Hodgkin–Huxley model requires the addition of a slow-modulation due to Ca inactivation dynamics. We accommodate this extra inactivation channel by first considering the two-dimensional “reduced” excitation model as described by Morris-Lecar [37]

$$C_{mem}\frac{dV_i}{dt} = -I_{Ca_i} - I_{K_i} - I_{L_i} - I_{syn_{ij}} \tag{2}$$

where $i, j = 0 \ldots 3$, and

$$\begin{aligned} I_{Ca_i} &= m_{\infty_i} g_{Ca_i} (V_i - E_{Ca_i}) \\ I_{K_i} &= w_i g_{K_i} (V_i - E_{K_i}) \\ I_{L_i} &= g_{L_i} (V_i - E_{L_i}) \\ I_{syn_{ij}} &= r_{ij} g_{syn_{ij}} (V_i - E_{syn_{ij}}). \end{aligned} \tag{3}$$

We then reintroduce the variable $h_i$ as a multiplicative term in the calcium conductance in (3), modeling the calcium recovery rather than calcium inactivation, on a slower timescale spanning several action potentials. We also revert to the cubic form of fast Ca (Na) activation in the Hodgkin–Huxley model, of the form (1). We show that we can adapt this model (1) to reproduce rich spiking and bursting dynamics, with only changes in the conductance and channel kinetics, illustrated in Fig. 1 and described below.

### B. Channel Kinetics

The neuron channel gating variables are modeled by a rate-based first-order approximation to the kinetics governing the random opening and closing of membrane channels for any of the gating variables $x$ (e.g., $m$, $h$, $n$, $w$)

$$\frac{dx_i}{dt} = \alpha_{x_i}(1 - x_i) - \beta_{x_i} x_i \tag{4}$$

where each channel variable denotes the fractions of corresponding channel gates in the open state, and where the $\alpha$ and $\beta$ parameters are the corresponding voltage-dependent opening and closing rates. The channel variables can be equivalently expressed as

$$\tau_{x_i}\frac{dx_i}{dt} = x_{\infty_i} - x_i \tag{5}$$

with asymptotes $x_{\infty_i} = \alpha_{x_i}/(\alpha_{x_i} + \beta_{x_i})$ and time constants $\tau_{x_i} = 1/(\alpha_{x_i} + \beta_{x_i})$.

We model each of the opening and closing channel kinetics in the *NeuroDyn* system using the seven-point sigmoidal regression functions implemented as cascaded differential pairs. As described in [31], we use a least squares fit regression technique to determine the appropriate current biases to fit the generalized channel kinetic functions.

Simulation data was obtained by implementing the models described using MATLAB. The simulation and circuit measurement data illustrating the neural spiking behavior before and after the inclusion of the slow inactivation channel are shown in Fig. 2 and Fig. 3, respectively. Neural spiking behavior before the inclusion of the slow inactivation channel is realized by setting the $h$ gating variable channel kinetics with voltage-independent opening and closing rates. The slow inactivation channel is realized by implementing the the $h$ gating variable channel kinetics as a slow inactivation channel.

## IV. Spiking to Bursting Behaviors

We calculate the ISI histogram for each burst of spikes over the variation of a single parameter $g_w$ governing calcium recovery [17] for both simulation and circuit measurement data as displayed in Fig. 4 and Fig. 5. We observe consistent spiking behavior over a wide regime of neural dynamics. For $g_w$ low conductance values, the neuron spikes and is followed by subthreshold oscillations. As the $g_w$ conductance value is increased, the neuron spikes and the following subthreshold oscillations are more pronounced. And when the $g_w$ conductance value is further increased, the neuron spikes in a bursting manner. When the $g_w$ conductance value is further increased, the number of subsequent bursting spikes is reduced as we observed quadruplets then triplets then doublets and finally single neuron spikes. Mismatch between simulation and measurement results can be attributed to circuit noise which manifests as fluctuations in spike and burst rates as well as the number of spikes per burst.

## V. Additional Spiking Behaviors

### A. Phasic Spiking

Phasic spiking dynamics refers to the property of certain neurons to respond with a single action potential corresponding to the onset of an applied excitatory current input pulse. We present simulation and circuit measurement results in Fig. 6. We demonstrate phasic spiking dynamics by increasing values of $\tau_n$ with respect to $\tau_h$ from the tonic spiking model channel kinetic rate parameters.

### B. Spike Frequency Adaptation

Spike frequency adaptation refers to the property of certain neurons to spike with greater frequency at the onset of an applied pulse of current and decrease in spike frequency through the duration of the pulse. We present simulation and circuit measurement results for spike frequency adaptation dynamics in Fig. 7. We decrease values of $\tau_h$ with respect to $\tau_n$ in order to more readily observe spike frequency adaptation dynamics.

### C. Neural Excitability

**1) Class 1 Neural Excitability—**Class 1 neural excitability refers to the property of certain neurons to respond to an applied excitatory current ramp with a train of action potentials. The frequency of the action potentials starts from an arbitrarily low frequency and increases in frequency through the duration of the applied ramp input resulting a large band of frequency response. We present simulation and circuit measurement data for class 1 neural excitability in Fig. 8.

**2) Class 2 Neural Excitability—**In contrast, neurons that exhibit class 2 neural excitability display a narrow band of frequencies in response to an applied excitatory current ramp. Class 2 excitability is further distinguished from class 1 excitability by the high frequency of its initial response to the applied current ramp. We present simulation and circuit measurement data for class 2 neural excitability in Fig. 9. We vary the dynamical profile of gating variable $n$ to decrease the values of $\tau_n$ governing $K^+$ channel dynamics in order to achieve class 2 neural excitability dynamics. The decrease in $\tau_n$ results in a corresponding decrease in refractory period between action potentials.

**3) Transition from Class 1 to Class 2 Neural Excitability Dynamics—**We calculate the ISI histogram for each ramp response over the variation of a set of parameters governing $\tau_n$ and corresponding to $K^+$ channel dynamics for both simulation and circuit measurement data as displayed in Fig. 10 and Fig. 11. For low values of $\tau_n$, the neuron

responds with a narrow band of frequencies at relatively low ISI characteristic of class 2 excitable neural dynamics. As the value for $\tau_n$ is increased, the refractory period between action potentials increases and becomes more pronounced at the onset of the current ramp input. This results in a broader band of frequency response over the course of the applied current ramp input. As the value for $\tau_n$ is further increased, the band of frequency responses continues to increase as is characteristic of class 1 excitable neural dynamics.

When current is injected into the HH model, there is a threshold where the firing rate jumps from zero to some finite value. The addition of an "A-current" $K^+$ conductance to the model makes the input-output curve contiguous as first shown by Connor and Stevens [38]. In the augmented model, the deinactivation rate of the "A-current" limits the rise time of the membrane potential between action potentials.

## VI. Conclusion

Previous studies [39] have shown intrinsically bursting neural dynamics implemented with extensions to the HH model requiring more gating variables. Other models are capable of emulating intrinsic bursting neural dynamics, such as Izhikevich's simple model [20] which uses just two dynamical variables and Mihalas-Niebur's neural model [21] which uses three dynamical variables to also govern threshold adaptation. Here we have presented red an extended HH-ML model that reproduces a variety of neural dynamics in three dynamical variables that directly account for the biophysics of membranes and channels over an extended range of time scales in the *NeuroDyn* neural emulation platform. The neural dynamics has been implemented with individual control over biophysical parameters governing the dynamical profiles of the opening and closing channel rates, reversal potential, and conductance. Intrinsic noise due to analog circuit implementation results in quantitative and qualitative changes in the neuronal dynamics including changes in the onset and regularity of spiking and bursting patterns, although we observed general qualitative correspondence between simulations and circuit experiments. Similarly, noise from thermal, stochastic, and other sources observed in *in vivo* recordings play an important role in the dynamics of neuronal activity [40], [41]. Thus, the noise inherently present in the analog circuits adds to the biological realism of the implementation avoiding quantization and periodicity artifacts commonly encountered in noise-free digital implementations.

## Acknowledgments

This work was supported by NIH R01AG029681, DARPA HR0011-10-C-0032 (NeoVision2) with Evolved Machines, and Qual-comm. This paper was recommended by Associate Editor Julius Georgiou.

The authors would like to thank S. Deiss and M. Chi for help with the experimental setup, and the MOSIS Educational Program for fabricating the chip. The authors also benefited from interactions with participants at the NSF Workshop on Neuromorphic Cognition Engineering in Telluride, CO.

## References

1. Satyanarayana S, Tsividis YP, Graf HP. A reconfigurable VLSI neural network. J Solid State Circuits. Jan.1992 27(1):67.
2. Indiveri G, Chicca E, Douglas R. A VLSI array to low-power spiking neurons and bistable synapses with spike-timing dependent plasticity. IEEE Trans Neural Netw. Jan; 2006 17(1):211–221. [PubMed: 16526488]
3. Simoni MF, Cymbalyuk GS, Sorensen ME, Calabrese RL, DeWerth SP. A multiconductance silicon neuron with biologically matched dynamics. IEEE Trans Biomed Eng. Feb; 2004 51(2):342–354. [PubMed: 14765707]

4. Simoni MF, DeWerth SP. Two-dimensional variation of bursting properties in a silicon-neuron half-center oscillator. IEEE Trans Neural Syst Rehabil Eng. Sep; 2006 14(3):281–289. [PubMed: 17009487]
5. Vogelstein RJ, Mallik U, Vogelstein JT, Cauwenberghs G. Dynamically reconfigurable silicon array of spiking neurons with conductance-based synapses. IEEE Trans Neural Netw. Jan; 2007 18(1): 253–265. [PubMed: 17278476]
6. Badoni, D.; Giulioni, M.; Dante, V.; Del Giudice, P. An aVLSI recurrent network of spiking neurons with reconfigurable and plastic synapses. Proc. IEEE Int. Symp. Circuits and Systems; 2006. p. 1227-1230.
7. Saighi, S.; Bornat, Y.; Tomas, J.; Renaud, S. Neuromimetic ICs and system for parameters extraction in biological neuron models. Proc. IEEE Int. Symp. Circuits and Systems; 2006. p. 4207-4211.
8. Saighi S, Bornat Y, Tomas J, LeMasson G, Renaud S. A library of analog operators based on the Hodgkin–Huxley formalism for the design of tunable, real-time silicon neurons. IEEE Trans Biomed Circuits Syst. Feb; 2011 5(1):3–19.
9. Tenore, F.; Vogelstein, RJ.; Etienne-Cummings, R.; Cauwenberghs, G.; Hasler, P. A floating-gate programmable array of silicon neurons for central pattern generating networks. Proc. IEEE Int. Symp. Circuits and Systems; 2006. p. 3157-3160.
10. Basu A, Ramakrishnan S, Petre C, Koziol S, Brink S, Hasler P. Neural Dynamics in Reconfigurable Silicon. IEEE Trans Biomed Circuits Syst. Oct; 2010 4(5):311–319.
11. Simoni MF, Cymbalyuk GS, Sorensen ME, Calabrese RL, DeWeerth SP. A multiconductance silicon neuron with biologically matched dynamics. IEEE Trans Biomed Eng. Feb; 2004 51(2): 342–354. [PubMed: 14765707]
12. Doi, S.; Onoda, Y.; Kumagai, S. Parameter estimation of various Hodgkin–Huxley-type neuronal models using a gradient-descent learning method. Proc. 41th SICE Annu. Conf; 2002. p. 1685-1688.
13. Buhry L, Grassia F, Giremus A, Grivel E, Renaud S, Saighi S. Automated parameter estimation of the Hodgkin–Huxley model using the differential evolution algorithm: Application to neuromimetic analog integrated circuits. Neural Comput. 2011 accepted for publication.
14. Russell A, Orchard G, Dong Y, Mihalas S, Niebur E, Tapson J, Etienne-Cummings R. Optimization methods for spiking neurons and networks. IEEE Trans Neural Netw. Dec; 2010 21(12):1950–1962. [PubMed: 20959265]
15. Neftci E, Chicca E, Indiveri G, Douglas R. A systematic method for configuring VLSI networks of spiking neurons. Neural Comput. 2011accepted for publication
16. Destexhe A, Mainen ZF, Sejnowski TJ. Synthesis of models for excitable membranes, synaptic transmission and neuromodulation using a common kinetic formalism. J Comp Neurosci. 1994; 1:195–230.
17. Izhikevich, E. Dynamical Systems in Neuroscience: The Geometry of Excitability and Bursting. Cambridge, MA: MIT Press; 2006.
18. Harris-Warrick, RM.; Marder, E.; Selverston, AI.; Moulin, M. Dynamic Biological Networks: The Stomatogastric Nervous System. Cambridge, MA: MIT Press; 1992.
19. Sejnowski TJ, Destexhe A. Why do we sleep? Brain Res. 2000; 886(1–2):208–223. [PubMed: 11119697]
20. Izhikevich EM. Simple model of spiking neurons. IEEE Trans Neural Netw. Nov; 2003 14(6): 1569–1572. [PubMed: 18244602]
21. Mihalas S, Niebur E. A generalized linear integrate-and-fire neural model produces diverse spiking behaviors. Neural Comput. 2009; 21:704–718. [PubMed: 18928368]
22. van Schaik, A.; Jin, C.; McEwan, A.; Hamilton, TJ. A log-domain implementation of the Izhikevich neuron model. Proc. IEEE Int. Symp. Circuits and Systems; 2010. p. 4253-4256.
23. Rangan, V.; Ghosh, A.; Aparin, V.; Cauwenberghs, G. A subthreshold aVLSI implementation of the Izhikevich simple neuron model. Proc. Int. Conf. IEEE Engineering in Medicine and Biology Society; 2010. p. 4164-4167.
24. Wijekoon, JHB.; Dudek, P. Spiking and bursting firing patterns of a compact VLSI cortical neuron circuit. Proc. Int. Joint Conf. Neural Networks; 2007. p. 1332-1337.

25. Folowosele, F.; Harrison, A.; Cassidy, A.; Andreou, A.; Etienne-Cummings, R.; Mihalas, S.; Niebur, E.; Hamilton, T. A switched capacitor implementation of the generalized linear integrate-and-fire neuron. Proc. IEEE Int. Symp. Circuits and Systems; 2009. p. 2149-2152.
26. Indiveri G, Linares-Barranco B, Hamilton TJ, van Schaik A, Etienne-Cummings R, Delbruck T, Liu SC, Dudek P, Hafliger P, Renaud S, Schemmel J, Cauwenberghs G, Arthur J, Hynna K, Folowosele F, Saighi S, Serrano-Gotarredona T, Wijekoon J, Wang Y, Boahen K. Neuromorphic silicon neuron circuits. Frontiers in Neuroscience. 2011; 5
27. Basu A, Petre C, Hasler P. Dynamics and bifurcations in a silicon neuron. IEEE Trans Biomed Circuits Syst. Oct; 2010 4(5):320–328.
28. Yu, T.; Sejnowski, TJ.; Cauwenberghs, G. Biophysical neural spiking and bursting dynamics in reconfigurable analog VLSI. Proc. IEEE Biomedical Circuits and Systems Conf; 2010. p. 186
29. Yu, T.; Cauwenberghs, G. Analog VLSI neuromorphic network with programmable membrane channel kinetics. Proc. IEEE Int. Symp. Circuits and Systems; 2009. p. 349-352.
30. Yu, T.; Cauwenberghs, G. Biophysical synaptic dynamics in an analog VLSI network of Hodgkin–Huxley neurons. Proc. Int. Conf. IEEE Engineering in Medicine and Biology Society; 2009. p. 3335-3338.
31. Yu T, Cauwenberghs G. Analog VLSI Biophysical Neurons and Synapses With Programmable Membrane Channel Kinetics. IEEE Trans Biomed Circuits Syst. May; 2010 4(3):139–148.
32. Prescott SA, Ratte S, Koninck YD, Sejnowski TJ. Pyramidal neurons switch from integrators in vitro to resonators under in vivo-like conditions. J Neurophysiol. Dec.2008 100:3030–3042. [PubMed: 18829848]
33. Greenwald E, Mollazadeh M, Hu C, Tang W, Culurciello E, Thakor NV. A VLSI neural monitoring system with ultra-wideband telemetry for awake behaving subjects. IEEE Trans Biomed Circuits Syst. Apr; 2011 5(2):112–119.
34. O'Driscoll S, Shenoy KV, Meng TH. Adaptive resolution ADC array for an implantable neural sensor. IEEE Trans Biomed Circuits Syst. Apr; 2011 5(2):120–130.
35. Narasimhan S, Chiel HJ, Bhunia S. Ultra-low-power and robust digital-signal-processing hardware for implantable neural interface microsystems. IEEE Trans Biomed Circuits Syst. Apr; 2011 5(2): 169–178.
36. Hogdkin AL, Huxley AF. A quantitative description of membrane current and its application to conduction and excitation in nerve. J Physiol. 1952; 117:500–544. [PubMed: 12991237]
37. Morris C, Lecar H. Voltage oscillations in the barnacle giant muscle fiber. J Biophys. July.1981 35:193–213.
38. Connor JA, Stevens CF. Prediction of repetitive firing behavior from voltage clamp data on an isolated neurone soma. J Physiol. 1971; 213:31–53. [PubMed: 5575343]
39. Chay T. Modeling slowly bursting neurons via calcium store and voltage-independent calcium current. Neural Comput. 1996; 8:951–978. [PubMed: 8697230]
40. Manwani A, Koch C. Detecting and estimating signals in noisy cable structures, I: Neuronal noise sources. Neural Comput. 1999; 11:1797–1829. [PubMed: 10578033]
41. Padmanabhan K, Urban N. Intrinsic biophysical diversity decorrelates neuronal firing while increasing information content. Nature Neurosci. 2010; 13:1276–1282. [PubMed: 20802489]

## Biographies

**Theodore Yu** (S'04) received the B.S. and M.S. degrees in electrical engineering from the California Institute of Technology, Pasadena in 2004 and 2005, respectively.

Currently, he is working towards the Ph.D. degree at the University of California, San Diego, in the electrical and computer engineering program. His research interests include neuromorphic analog VLSI models of neural and synaptic circuits, neuron-silicon interfaces, and circuit implementations of learning algorithms.

**Terrence J. Sejnowski** (SM'91–F'06) is the Francis Crick Professor at The Salk Institute for Biological Studies, where he directs the Computational Neurobiology Laboratory, an Investigator with the Howard Hughes Medical Institute, and a Professor of Biology and Computer Science and Engineering at the University of California, San Diego, where he is Co-Director of the Institute for Neural Computation. The long-range goal of his laboratory is to understand the computational resources of brains and to build linking principles from brain to behavior using computational models. This goal is being pursued with a combination of theoretical and experimental approaches at several levels of investigation ranging from the biophysical level to the systems level. His laboratory has developed new methods for analyzing the sources for electrical and magnetic signals recorded from the scalp and hemodynamic signals from functional brain imaging by blind separation using independent components analysis (ICA). He has authored over 300 scientific papers and 12 books, including *The Computational Brain* (MIT Press, 1994), with Patricia Churchland.

Dr. Sejnowski received the Wright Prize for Interdisciplinary research in 1996, the Hebb Prize from the International Neural Network Society in 1999, and the IEEE Neural Network Pioneer Award in 2002. He was elected an AAAS Fellow in 2006, to the Institute of Medicine in 2008, the National Academy of Sciences in 2010, and the National Academy of Engineering in 2011.

**Gert Cauwenberghs** (S'89–M'94–SM'04–F'11) received the M. Eng. degree in applied physics from the University of Brussels, Brussels, Belgium, in 1988, and the M.S. and Ph.D. degrees in electrical engineering from the California Institute of Technology, Pasadena, in 1989 and 1994, respectively.

Currently, he is a Professor of Bioengineering at the University of California, San Diego, where he codirects the Institute for Neural Computation, participates as a member of the Institute of Engineering in Medicine, and serves on the Computational Neuroscience

Executive Committee of the Department of Neurosciences graduate program. Previously, he was Professor of Electrical and Computer Engineering at Johns Hopkins University, Baltimore, MD, and Visiting Professor of Brain and Cognitive Science at the Massachusetts Institute of Technology, Cambridge. His research focuses on micropower biomedical instrumentation, neuron-silicon and brain-machine interfaces, neuromorphic engineering, and adaptive intelligent systems.

Dr. Cauwenberghs received the National Science Foundation Career Award in 1997, the ONR Young Investigator Award in 1999, and the Presidential Early Career Award for Scientists and Engineers in 2000. He was Francqui Fellow of the Belgian American Educational Foundation. He was a Distinguished Lecturer of the IEEE Circuits and Systems Society in 20022003. He continues to serve IEEE in a variety of roles, most recently cochairing the IEEE Biomedical Circuits and Systems Conference (BioCAS2011) and the technical program committee of the IEEE Engineering in Medicine and Biology Conference (EMBC2012), both held in San Diego. He is a Senior Editor for the IEEE Sensors Journal and the IEEE Journal on Emerging and Selected Topics in Circuits and Systems, and Editor-in-Chief of the IEEE Transactions on Biomedical Circuits and Systems.

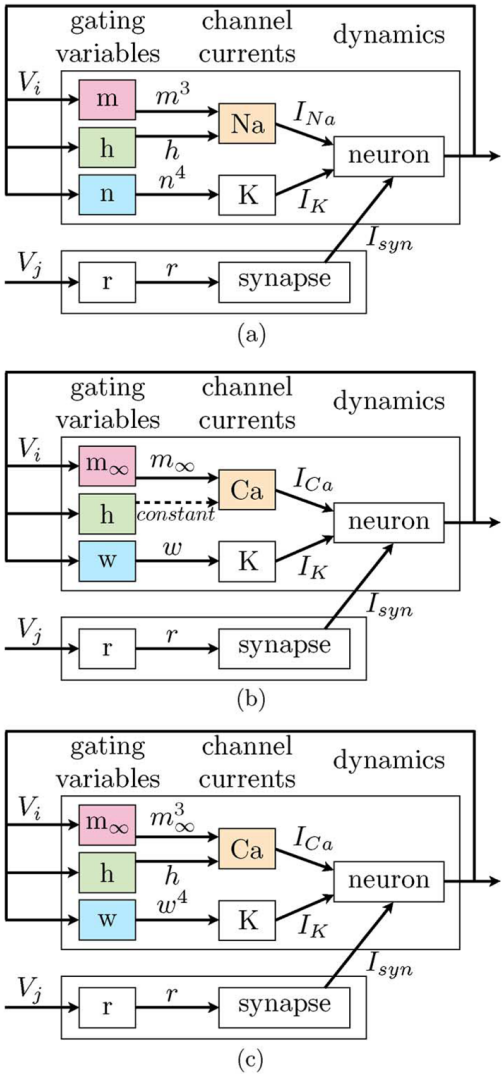


**Fig. 1.**

The *NeuroDyn* analog VLSI programmable neural emulation platform [29]–[31] is used to generate both tonic firing and intrinsic bursting dynamics using extensions on Hodgkin–Huxley and Morris-Lecar paradigms. (a) Hodgkin–Huxley. (b) Morris-Lecar. (c) extended Morris-Lecar and Hodgkin–Huxley.

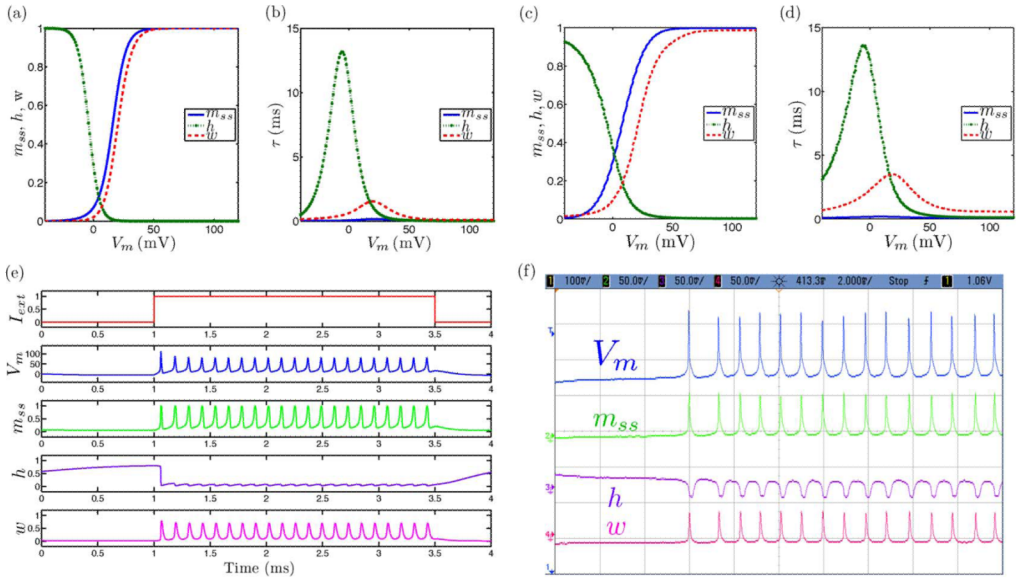


**Fig. 2.**

Tonic spiking neural dynamics in the ML model with the extension to include slow inactivation dynamics set as a constant parameter showing simulated and measured data for (a), (c) steady-state (in)activation dynamics, (b), (d) $\tau$ voltage-dependent dynamics, and (e), (f) membrane voltage and gating variable waveforms.

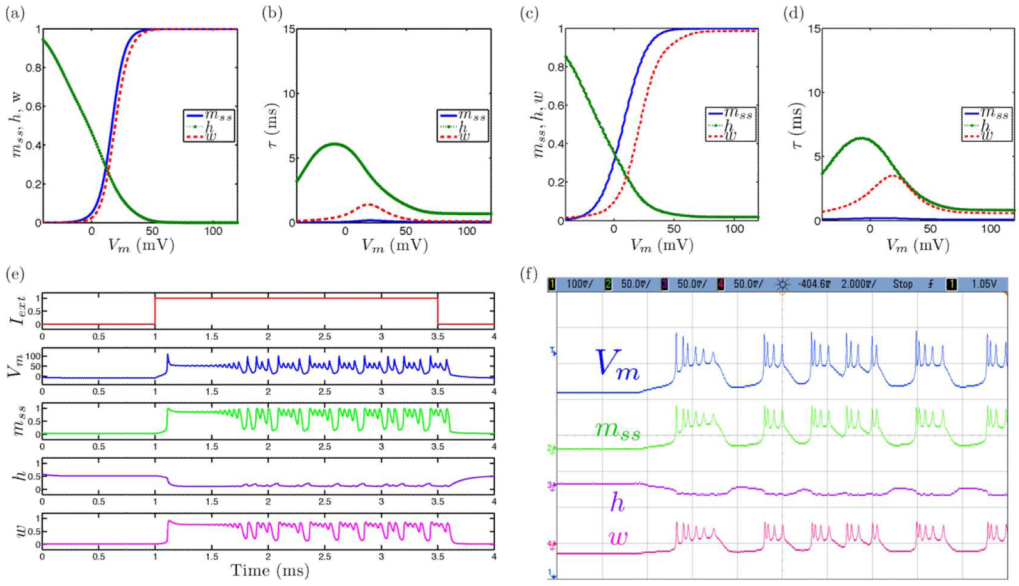


**Fig. 3.**

Tonic bursting neural dynamics in the ML model with an extension to include slow inactivation dynamics showing simulated and measured data for (a), (c) steady-state (in)activation dynamics, (b), (d) $\tau$ voltage-dependent dynamics, and (e), (f) membrane voltage and gating variable waveforms.

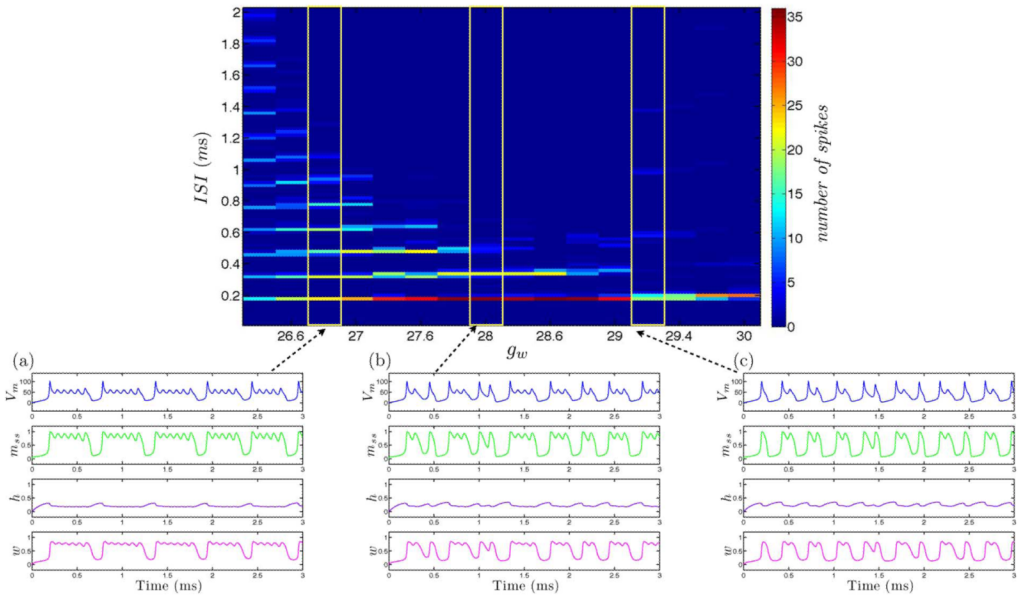


**Fig. 4.**

Simulated tonic bursting neuron with variation of a single conductance parameter $g_w$ governing calcium recovery with increasing values from (a) to (c).

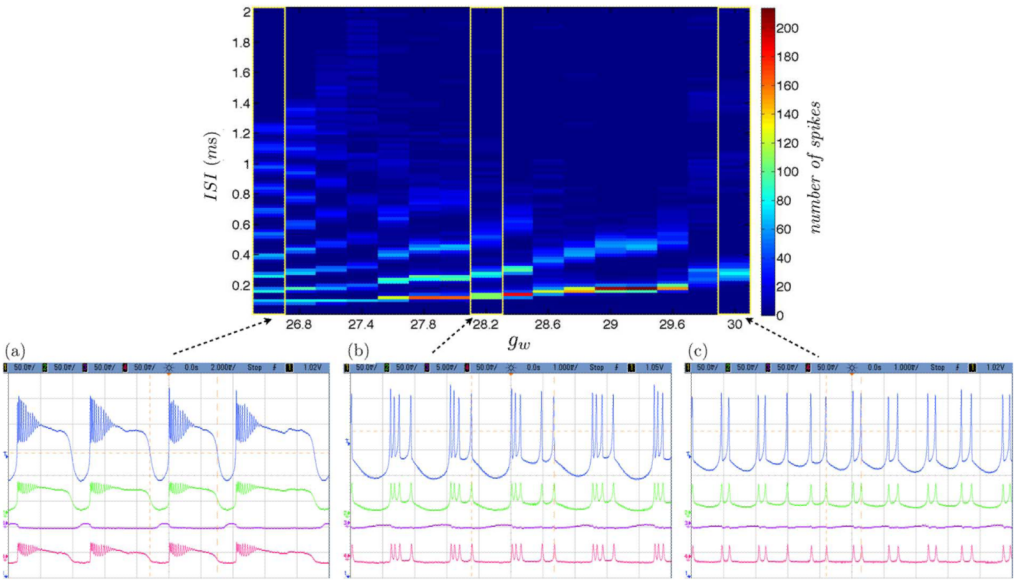


**Fig. 5.**
Measured tonic bursting neuron with variation of a single conductance parameter $g_w$ governing calcium recovery with increasing values from (a) to (c).

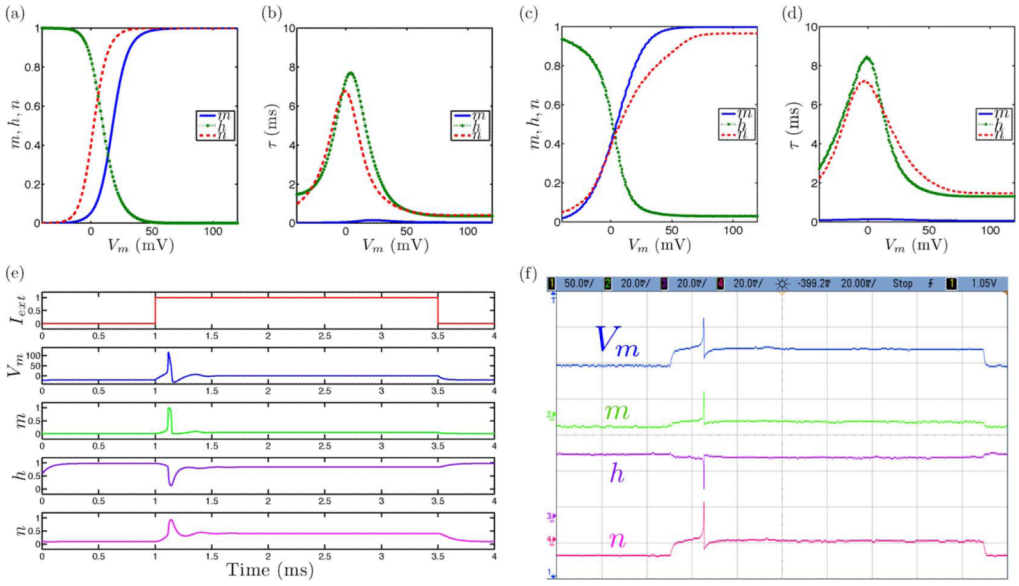


**Fig. 6.**

Phasic spiking neural dynamics with simulated and measured data for (a), (c) steady-state (in)activation dynamics, (b), (d) $\tau$ voltage-dependent dynamics, and (e), (f) membrane voltage and gating variable waveforms.

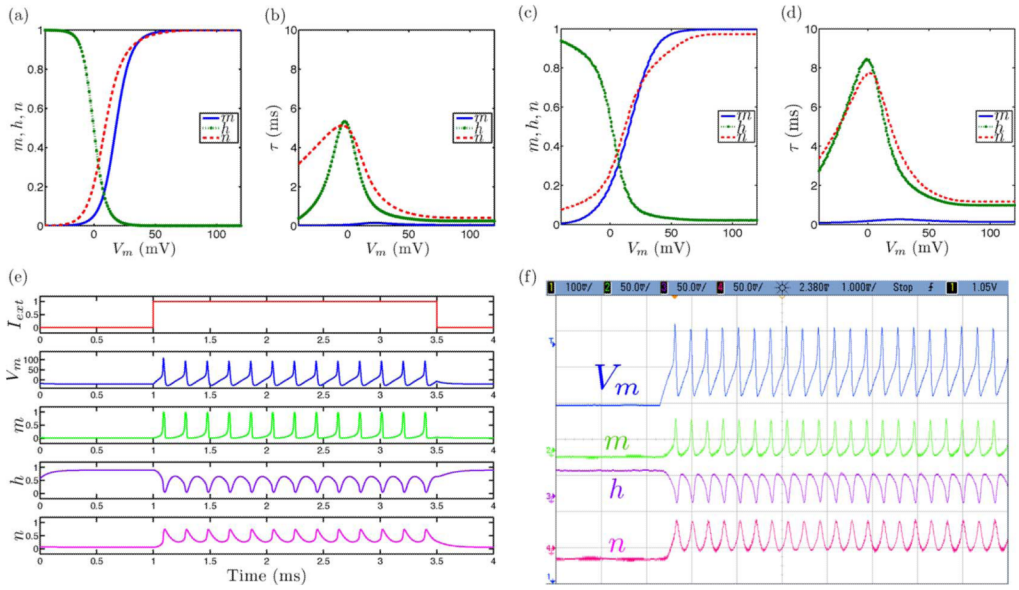


**Fig. 7.**

Spike frequency adaptation neural dynamics with simulated and measured data for (a), (c) steady-state (in)activation dynamics, (b), (d) $\tau$ voltage-dependent dynamics, and (e), (f) membrane voltage and gating variable waveforms.

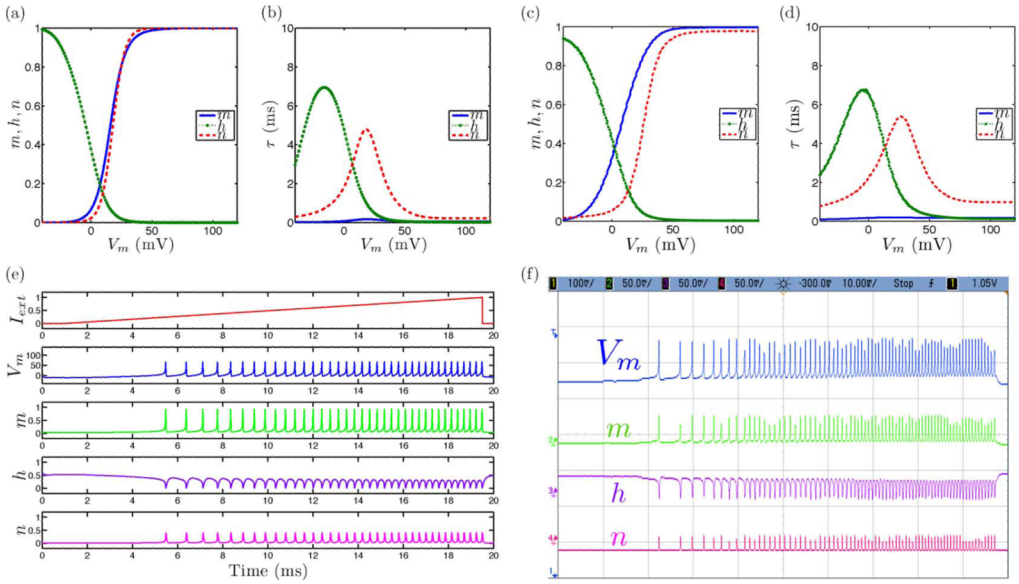


**Fig. 8.**

Class 1 excitable neural dynamics with simulated and measured data for (a), (c) steady-state (in)activation dynamics, (b), (d) $\tau$ voltage-dependent dynamics, and (e), (f) membrane voltage and gating variable waveforms.

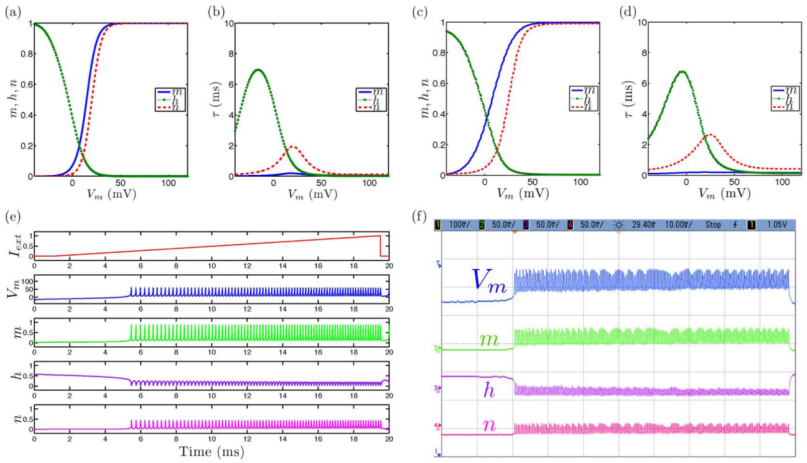


**Fig. 9.**

Class 2 excitable neural dynamics with simulated and measured data for (a), (c) steady-state (in)activation dynamics, (b), (d) $\tau$ voltage-dependent dynamics, and (e), (f) membrane voltage and gating variable waveforms.

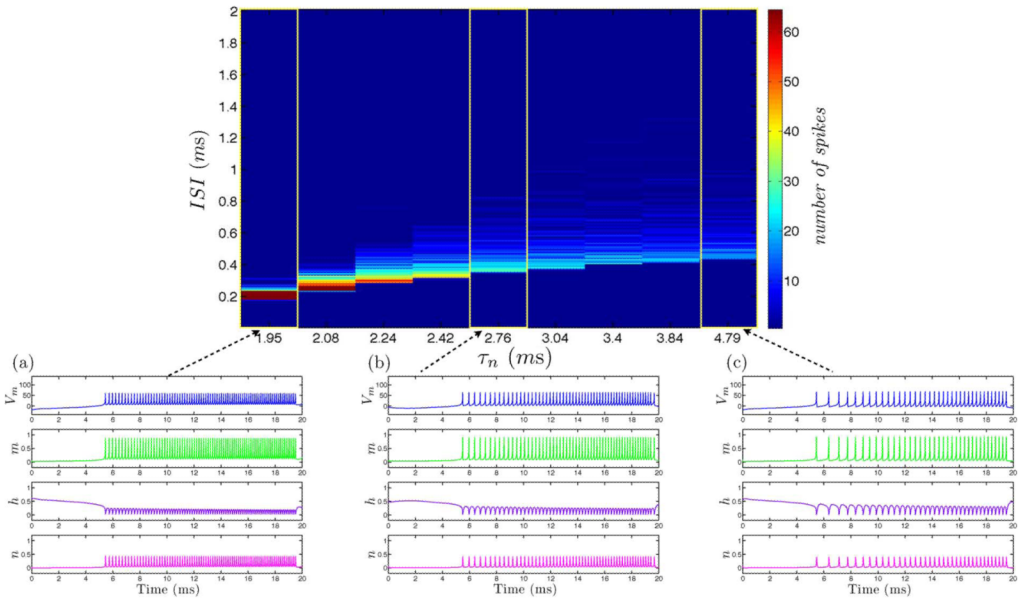


**Fig. 10.**

ISI Histogram of increasing values $\tau_n$ for from (a) to (c) governing $K^+$ channel dynamics of simulations between class 1 and class 2 excitable neural dynamics.

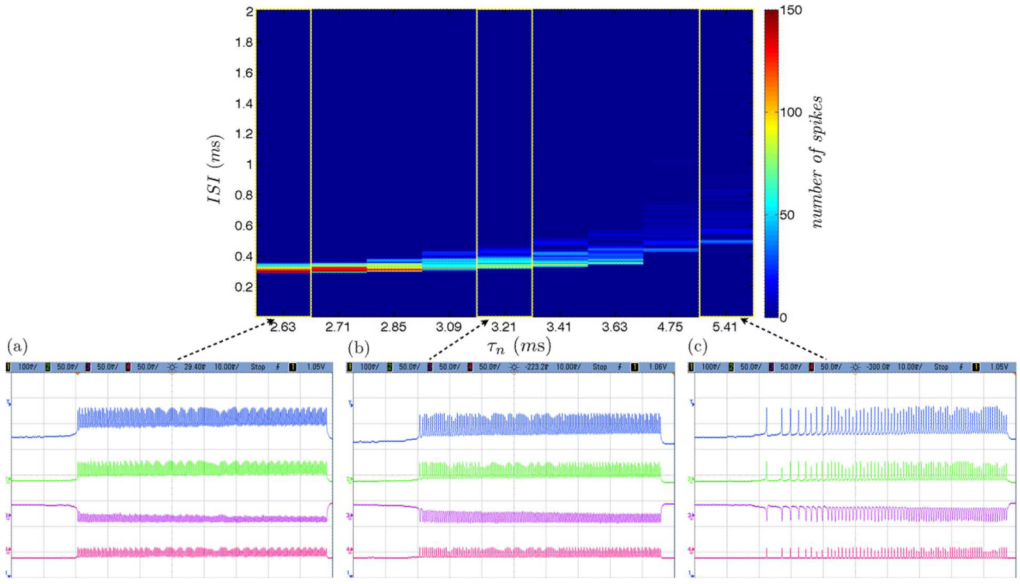


**Fig. 11.**

ISI Histogram of increasing values for $\tau_n$ from (a) to (c) governing $K^+$ channel dynamics of measurements between class 1 and class 2 excitable neural dynamics.